



This is a repository copy of *Bespoke diblock copolymer nanoparticles enable production of relatively stable oil-in-water Pickering nanoemulsions*.

White Rose Research Online URL for this paper:

<https://eprints.whiterose.ac.uk/122513/>

Version: Published Version

Article:

Thompson, K.L., Cinotti, N., Jones, E.R. et al. (3 more authors) (2017) Bespoke diblock copolymer nanoparticles enable production of relatively stable oil-in-water Pickering nanoemulsions. *Langmuir*, 33 (44). pp. 12616-12623. ISSN 0743-7463

<https://doi.org/10.1021/acs.langmuir.7b02267>

Reuse

This article is distributed under the terms of the Creative Commons Attribution (CC BY) licence. This licence allows you to distribute, remix, tweak, and build upon the work, even commercially, as long as you credit the authors for the original work. More information and the full terms of the licence here:

<https://creativecommons.org/licenses/>

Takedown

If you consider content in White Rose Research Online to be in breach of UK law, please notify us by emailing eprints@whiterose.ac.uk including the URL of the record and the reason for the withdrawal request.



eprints@whiterose.ac.uk
<https://eprints.whiterose.ac.uk/>

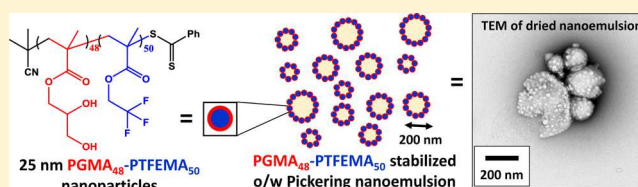
Bespoke Diblock Copolymer Nanoparticles Enable the Production of Relatively Stable Oil-in-Water Pickering Nanoemulsions

Kate L. Thompson,* Natacha Cinotti, Elizabeth R. Jones, Charlotte J. Mable, Patrick W. Fowler, and Steven P. Armes*[✉]

Department of Chemistry, University of Sheffield, Dainton Building, Brook Hill, Sheffield, South Yorkshire S3 7HF, U.K.

Supporting Information

ABSTRACT: Sterically stabilized diblock copolymer nanoparticles with an intensity-average diameter of 25 nm are prepared in the form of a concentrated aqueous dispersion using polymerization-induced self-assembly (PISA). The addition of *n*-dodecane followed by high-shear homogenization produces *n*-dodecane-in-water Pickering macroemulsions of 22–46 μm diameter. If the nanoparticles are present in sufficient excess, then subsequent processing using a high-pressure microfluidizer leads to the formation of Pickering nanoemulsions with a mean oil droplet diameter below 200 nm. The size of these Pickering nanoemulsions can be tuned by systematically varying the nanoparticle concentration, applied pressure, number of passes, and oil volume fraction. High-internal-phase emulsions can also be achieved by increasing the *n*-dodecane volume fraction up to 0.80. TEM studies of (dried) *n*-dodecane droplets confirm the presence of intact nanoparticles and suggest a relatively high surface coverage, which is consistent with model packing calculations based on radius ratios. Such Pickering nanoemulsions proved to be surprisingly stable with respect to Ostwald ripening, with no significant change in the mean DLS droplet diameter after storage for approximately 4 months at 20 $^{\circ}\text{C}$.



INTRODUCTION

Pickering emulsions are oil or water droplets stabilized solely by solid particles.^{1,2} Their excellent long-term stability is attributed to strong irreversible particle adsorption at the oil–water interface.³ Many types of colloidal particles can be used to prepare Pickering emulsions, including silica, gold sols, magnetite, microgels, and latexes.³ However, relatively large droplets with mean diameters of 10–100 μm are typically obtained unless surfactant is added to lower the surface tension of the oil or modify the particle wettability.³ In principle, Pickering emulsions provide access to highly reproducible nonfoaming formulations with minimal skin irritancy.³

Recently, various examples of so-called nanoemulsions have been reported^{4–8} for which the mean droplet diameter is in the 50 to 200 nm range. (Somewhat confusingly, the older literature uses the term miniemulsions to describe similar systems.^{9,10}) Such fine droplets mean that gravitational creaming or sedimentation become negligible even over relatively long time scales. Moreover, the much higher droplet surface area leads to more active formulations that are potentially advantageous for cosmetics,⁶ agrochemicals,^{11,12} drug delivery,⁷ and food manufacturing applications.^{8,13,14} Copolymer- or surfactant-stabilized nanoemulsions can be prepared using energy-intensive methods such as high-shear homogenization,¹¹ microfluidization,¹² or ultrasonication.⁷ Alternatively, low-energy routes utilize a phase inversion temperature (PIT)^{15–17} or an emulsion inversion point (EIP).¹⁸ However, there have been remarkably few studies on Pickering nanoemulsions.^{19,20} Of particular relevance to the

present study, Persson et al.⁵ utilized a high-pressure microfluidizer to prepare a series of oil-in-water emulsions of 100–200 nm diameter using a 7 nm silica sol. Unfortunately, Ostwald ripening is very common for nanoemulsions, even for oils exhibiting relatively low solubility in the aqueous continuous phase.¹⁴ Indeed, droplet growth was observed by Persson et al.⁵ for both *cis*-decalin and a series of *n*-alkanes (including *n*-dodecane). On the other hand, squalene droplets exhibited much better long-term stability, because this particular oil has extremely low water solubility.⁵ Cheong and co-workers²¹ used β -cyclodextrin particles to prepare oil-in-water nanoemulsions with a mean droplet diameter of 156 nm. However, both sodium caseinate and Tween 20 were required as costabilizers for this formulation. Similarly, Glatter and coworkers²² obtained Pickering nanoemulsions via ultrasonics using a 10 nm silica sol, but again this approach required the addition of oleic acid to modify the surface wettability of the silica nanoparticles.

The recent development of polymerization-induced self-assembly (PISA) has enabled the highly convenient synthesis of well-defined sterically stabilized spherical diblock copolymer nanoparticles of 20–25 nm diameter directly in the form of concentrated aqueous dispersions.^{23–27} This is important, because the stabilization of Pickering (nano)emulsions normally requires (nano)particles at least 5–10 times smaller

Received: June 30, 2017

Revised: October 9, 2017

Published: October 12, 2017

than the mean droplet diameter.^{5,28–32} Herein, we demonstrate that PISA provides new opportunities for the rational design of bespoke organic nanoparticle emulsifiers to produce highly stable oil-in-water Pickering nanoemulsions in the absence of any other additives using a scalable emulsification protocol. More specifically, *n*-dodecane-in-water Pickering nanoemulsions can be prepared using an LV1 microfluidizer (Microfluidics, USA). The effect of varying the number of passes through the microfluidizer, the applied pressure, the initial copolymer nanoparticle concentration, the oil volume fraction, and the copolymer particle diameter is systematically investigated. The final nanoemulsions are characterized in terms of their droplet diameters, the nature of the adsorbed nanoparticle layer, and their long-term stability. Moreover, a simple packing model provides invoked to provide useful estimates of the number of adsorbed nanoparticles per oil droplet.

EXPERIMENTAL SECTION

Materials. Glycerol monomethacrylate (99.8% purity) was obtained from GEO Specialty Chemicals (Hythe, U.K.) and was used as received. 2-Cyano-2-propyl benzodithioate, 2,2,2-trifluoroethyl methacrylate, 4,4'-azobis(4-cyanopentanoic acid) (ACVA), fluorescein *O*-methacrylate (FluMA), *n*-dodecane, dichloromethane, and deuterium oxide were purchased from Aldrich (U.K.) and were used as received unless otherwise stated. Ethanol and DMF were purchased from VWR Chemicals (U.K.).

Synthesis of Poly(glycerol monomethacrylate) Macro-CTA via RAFT Solution Polymerization of Glycerol Monomethacrylate in Ethanol. A PGMA₄₈ macro-CTA (hereafter denoted as PGMA₄₈) was synthesized via RAFT polymerization of glycerol monomethacrylate in ethanol at 70 °C, as described previously.^{24,33} ¹H NMR studies indicated a mean degree of polymerization of 48 via end-group analysis. (The integrated aromatic RAFT end-group signals at 7.1–7.4 ppm were compared to those of the two oxymethylene protons at 3.5–4.4 ppm.) DMF GPC studies indicated a M_n of 12 700 g mol⁻¹ and a M_w/M_n of 1.17 relative to poly(methyl methacrylate) standards).

Synthesis of PGMA₄₈-PTFEMA₅₀ Diblock Copolymer Spherical Nanoparticles via RAFT Aqueous Emulsion Polymerization. PGMA₄₈-PTFEMA₅₀ diblock copolymer nanoparticles were synthesized as follows: PGMA₄₈ macro-CTA (2.830 g) and ACVA (0.020 g, 71.4 μmol; macro-CTA/ACVA molar ratio = 5.0) and water (52.65 g, 10% w/w) were weighed into a 100 mL round-bottomed flask, sealed with a rubber septum, and degassed with nitrogen for 30 min. TFEMA [2.54 mL, 17.8 mmol, target degree of polymerization (DP) = 50], which had been deoxygenated separately with nitrogen for 15 min, was then added to the solution under nitrogen and immersed in an oil bath set at 70 °C. The reaction solution was stirred for 20 h to ensure complete TFEMA monomer conversion, and the polymerization was quenched by exposure to air. ¹⁹F NMR spectroscopy analysis of the copolymer dissolved in *d*₆-acetone indicated less than 1% residual TFEMA monomer. DMF GPC studies indicated a M_n of 19 100 g mol⁻¹ and a M_w/M_n of 1.14 relative to poly(methyl methacrylate) standards).

Synthesis of Fluorescent PGMA₄₈-P(TFEMA₅₀-*stat*-FluMA₁) Spherical Nanoparticles via RAFT Aqueous Emulsion Copolymerization. PGMA₄₈-P(TFEMA₅₀-*stat*-FluMA₁) diblock copolymer nanoparticles were synthesized at 10% w/w solids as follows: PGMA₄₈ macro-CTA (0.98 g) and ACVA (0.0069 g, 24.7 μmol; macro-CTA/ACVA molar ratio = 5.0), FluMA (0.049 g, 12.4 μmol), and water (18.5 g) were weighed into a 100 mL round-bottomed flask, sealed with a rubber septum, and degassed with nitrogen for 30 min. TFEMA [0.88 mL, 6.18 mmol, target degree of polymerization (DP) = 50], which had been deoxygenated separately with nitrogen for 15 min, was then added to the solution under nitrogen and immersed in an oil bath set at 70 °C. The reaction solution was stirred for 20 h to ensure maximum comonomer conversion, and the polymerization was

quenched by exposure to air. Residual unreacted FluMA and TFEMA comonomers were removed via dialysis against water.

Preparation of PGMA₄₈-PTFEMA₅₀-Stabilized Pickering Macroemulsions Using High-Shear Homogenization. A PGMA₄₈-PTFEMA₅₀ aqueous dispersion (8.0 mL, 1.0–7.0% w/w) was added to a 14 mL glass vial and homogenized with 2.0 mL of *n*-dodecane for 2.0 min at 20 °C using an IKA Ultra-Turrax T-18 homogenizer with a 10 mm dispersing tool operating at 15 500 rpm. The resulting milky oil-in-water emulsion was then analyzed by optical microscopy and laser diffraction.

Preparation of PGMA₄₈-PTFEMA₅₀-Stabilized Pickering Nanoemulsions Using High-Pressure Microfluidization. A Pickering macroemulsion (1–6 mL, initial particle concentration in the aqueous phase = 1.0–7.0% w/w) was further processed using an LV1 low-volume microfluidizer processor (Microfluidics, USA). The pressure was adjusted to between 10 000 and 30 000 psi, and the number of passes through the LV1 was varied between 1 and 10.

Characterization. NMR Spectroscopy. ¹H and ¹⁹F NMR spectra were recorded in either *d*₆-acetone, D₂O, or CD₃OD using a Bruker Avance 400 spectrometer operating at 400 MHz.

Gel Permeation Chromatography (GPC). Molecular weights and dispersities were assessed using a gel permeation chromatography (GPC) instrument equipped with a Varian 290-LC pump injection module, a Varian 390-LC refractive index detector, and two Polymer Laboratories PL gel 5 μm mixed-C columns with a DMF mobile phase containing 0.01 M LiBr operating at 60 °C with a constant flow rate of 1.0 mL min⁻¹. DMSO was used as a flow rate marker, and calibration was achieved using a series of near-monodisperse poly(methyl methacrylate) standards.

Dynamic Light Scattering (DLS). Intensity-average hydrodynamic diameters were obtained by DLS using a Malvern Zetasizer NanoZS instrument at a fixed scattering angle of 173°. Aqueous dispersions of 0.01% w/w nanoparticles were analyzed using disposable cuvettes, and the results were averaged over three consecutive runs. The deionized water used to dilute each sample was ultrafiltered through a 0.20 μm membrane in order to remove extraneous dust.

Laser Diffraction. Each macroemulsion was sized using a Malvern Mastersizer 3000 instrument equipped with a hydro EV wet sample dispersion unit, a red HeNe laser operating at 633 nm, and a LED blue light source operating at 470 nm. The stirring rate was adjusted to 1500 rpm in order to avoid creaming of the emulsion during analysis. After each measurement, the cell was rinsed three times with deionized water; the glass walls of the cell were carefully wiped with lens-cleaning tissue to avoid cross-contamination, and the laser was aligned central to the detector prior to data acquisition.

Fluorescence Microscopy. Fluorescence microscopy images of PGMA₄₈-P(TFEMA₅₀-*stat*-FluMA₁)-stabilized Pickering macroemulsions were recorded using a Zeiss Axio Scope A1 microscope fitted with an AxioCam 1Cm1 monochrome camera. Droplets were imaged using LED illumination (LED module λ = 470 nm) and a Zeiss filter set 38 (excitation BP 470/40 nm and emission BP 525/50 nm). Images were captured and processed using ZEN lite 2012 software.

Transmission Electron Microscopy (TEM). Nanoemulsion dispersions were diluted fifty-fold at 20 °C to produce 0.20% w/w dispersions for transmission electron microscopy (TEM) studies. Copper/palladium TEM grids (Agar Scientific, U.K.) were surface coated in-house to produce a thin film of amorphous carbon. The grids were then plasma glow discharged for 30 s to create a hydrophilic surface. Individual samples (0.20% w/w, 12 μL) were adsorbed onto the freshly glow-discharged grids for 1 min and then blotted with filter paper to remove excess solution. To stain the copolymer aggregates, uranyl formate solution (0.75% w/w, 9 μL) was soaked on the sample-loaded grid for 20 s and then carefully blotted to remove excess stain. The grids were then dried using a vacuum hose. Imaging was performed at 100 kV using a Phillips CM100 instrument equipped with a Gatan 1 k CCD camera.

Results and Discussion. The sterically stabilized diblock copolymer nanoparticles used in this study were prepared as described previously using reversible addition–fragmentation chain transfer (RAFT) aqueous emulsion polymerization.³⁴ The water-soluble steric

stabilizer block was poly(glycerol monomethacrylate) [PGMA], and the water-insoluble core-forming block was poly(2,2,2-trifluoroethyl methacrylate) [PTFEMA].

Our previous experience of using PISA-synthesized diblock copolymer nano-objects to prepare Pickering emulsions confirmed that the hydrophobic character of the core-forming block is of critical importance.^{35,36} Selecting a weakly hydrophobic block such as poly(2-hydroxypropyl methacrylate) (PHPMA) means that the nanoparticles typically do not survive the high-shear homogenization conditions required for droplet formation. In such cases, the resulting emulsions are stabilized by individual copolymer chains generated from in situ dissociation of the original nanoparticles under high shear. However, we have recently confirmed that PGMA-PTFEMA nanoparticles remain intact when subjected to high-shear homogenization and hence can act as genuine Pickering emulsifiers.²⁵ PTFEMA was preferred over a cheaper hydrophobic block such as poly(benzyl methacrylate) because its semifluorinated nature confers significantly greater electron contrast for TEM studies.

A PGMA₄₈ chain-transfer agent prepared via RAFT solution polymerization²⁵ was chain-extended with TFEMA via RAFT aqueous emulsion polymerization^{25,37–39} to afford well-defined PGMA₄₈-PTFEMA₅₀ diblock copolymer nanoparticles (Figure 1A). A relatively short core-forming block was deliberately targeted to ensure that sufficiently small nanoparticles were produced via PISA, as required for the formation of Pickering nanoemulsions. Gel permeation chromatography analysis in DMF indicated a relatively narrow molecular weight distribution ($M_w/M_n = 1.14$) with minimal contamination by the PGMA₄₈ precursor, suggesting that both stages of this RAFT synthesis were well-controlled (Figure S1A).

The copolymer morphology was confirmed to be near-monodisperse spheres by transmission electron microscopy (TEM), with dynamic light scattering (DLS) indicating an intensity-average diameter of 25 nm (Figures 1B and S1B, respectively).

These PGMA₄₈-PTFEMA₅₀ nanoparticles were used as conventional Pickering emulsifiers to generate Pickering macroemulsions of approximately 40 μm diameter via high-shear homogenization using an UltraTurrax homogenizer. Figure 1C shows a fluorescence micrograph obtained for a typical macroemulsion prepared using 7.0% w/w fluorescein-labeled PGMA₄₈-PTFEMA₅₀ nanoparticles (one dye label per copolymer chain). This confirms that the nanoparticles adsorb at the *n*-dodecane/water interface. Figure S2 shows the variation in mean droplet diameter with nanoparticle concentration for this precursor macroemulsion at a fixed *n*-dodecane volume fraction of 0.20. The minimal change in droplet diameter is attributed to only a small fraction of the nanoparticles adsorbing onto the oil droplets during homogenization: a large excess remains in the aqueous continuous phase. This is important because these non-adsorbed nanoparticles are required to stabilize the substantial additional surface area that is generated when producing the much finer nanoemulsion droplets during the subsequent microfluidization processing step.

Effects of Applied Pressure and Number of Passes through the LV1. For initial microfluidization studies, an applied pressure of 20 000 psi was selected. A precursor macroemulsion prepared using 7.0% w/w PGMA₄₈-PTFEMA₅₀ nanoparticles was subjected to repeated passes through an LV1 microfluidizer, with the mean emulsion droplet diameter being assessed by DLS after each pass. A recent microfluidization study by Gupta and co-workers has shown that multiple passes are usually required to achieve the minimum droplet diameter.¹⁴

As expected, a significant reduction in emulsion droplet diameter was observed between the first and tenth passes (Figure 2A). We emphasize here that the reported mean emulsion droplet diameter includes the layer of adsorbed nanoparticles. In reality, the internal oil droplet diameter will be somewhat smaller (see later discussion). Visual inspection indicated incipient flocculation of the emulsion droplets after one to three passes. DLS studies indicate bimodal size distributions for the first seven passes, with unimodal size distributions being observed after eight passes (Figure S3). Although the final droplets obtained after ten passes are significantly smaller than those obtained for a typical Pickering emulsion,⁴⁰ such nanoemulsions

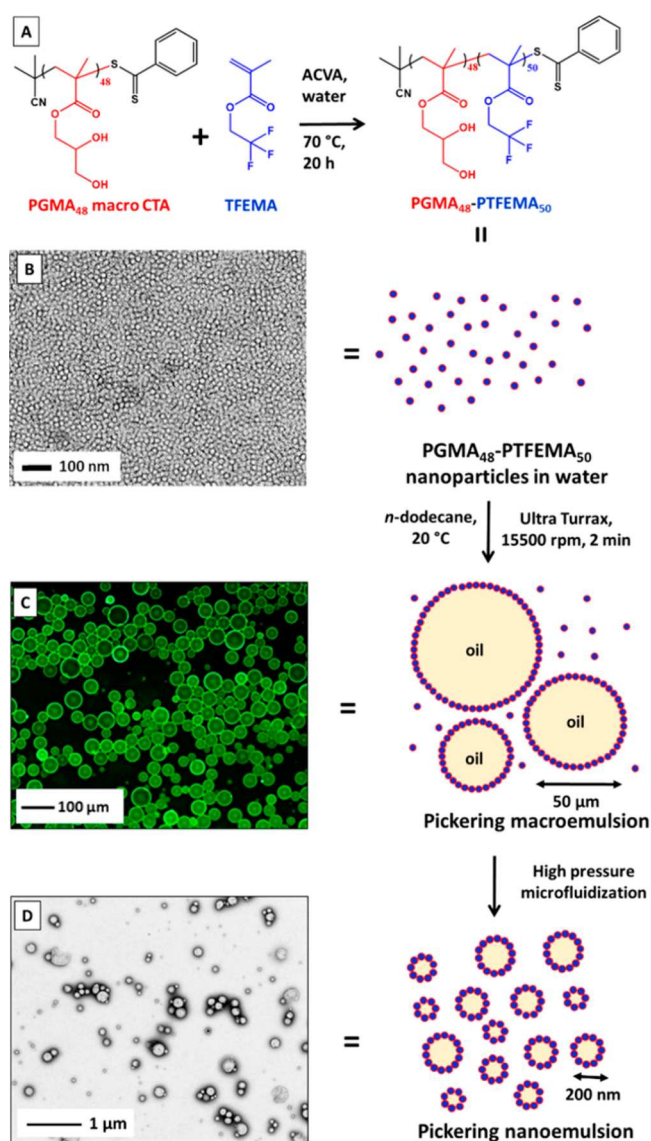


Figure 1. Schematic representation for the preparation of Pickering nanoemulsions described in this study. (A) Synthesis of PGMA₄₈-PTFEMA₅₀ nanoparticles of 25 nm diameter via RAFT emulsion polymerization using a PGMA₄₈ macro-CTA. (B) TEM image of the resulting sterically stabilized nanoparticles. (C) Fluorescence micrograph of the initial Pickering macroemulsion produced when excess nanoparticles are homogenized with *n*-dodecane for 2.0 min at 15 500 rpm. (D) This precursor macroemulsion was then further processed using the LV1 microfluidizer to give a Pickering nanoemulsion. (See the TEM image obtained after drying such droplets.)

remained highly turbid. (See digital photographs of a typical Pickering macroemulsion and its corresponding Pickering nanoemulsion in Figure S4.)

Having produced nanoemulsions with a mean diameter of 220 ± 85 nm at an applied pressure of 20 000 psi, the latter parameter was systematically varied to examine whether even finer nanoemulsions could be produced at higher pressures (Figure 2B). For a PGMA₄₈-PTFEMA₅₀ concentration of 7.0% w/w, an *n*-dodecane volume fraction of 0.20, and 10 passes, the mean droplet diameter could be reduced to just 133 nm at 30 000 psi, which is the maximum operating pressure for the LV1 microfluidizer. In addition, droplets prepared below 20 000 psi were significantly larger and considerably more polydisperse than those prepared at higher pressures.

Varying the Nanoparticle Concentration. The PGMA₄₈-PTFEMA₅₀ concentration was also systematically varied at a constant

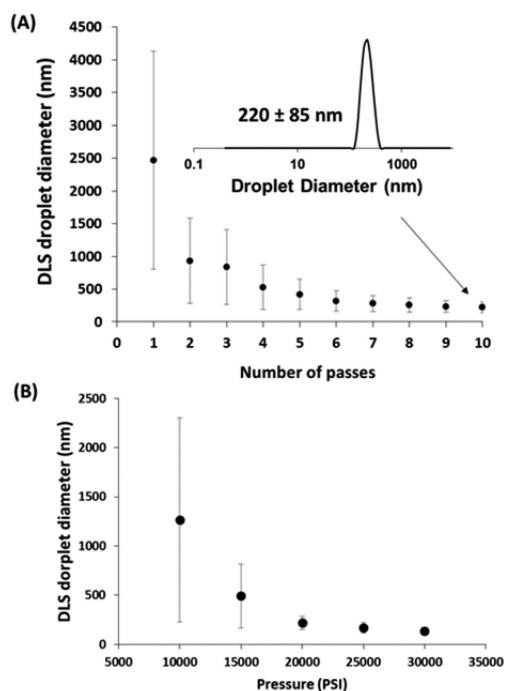


Figure 2. Systematic reduction in intensity-average droplet diameter observed for a Pickering nanoemulsion prepared at an *n*-dodecane volume fraction of 0.20 using 7.0% w/w PGMA₄₈-PTFEMA₅₀ nanoparticles with (A) an increasing number of passes through the LV1 microfluidizer at 20 000 psi and (B) increasing applied pressure for ten passes. Error bars represent the standard deviation of the droplet size distributions rather than the experimental error associated with repeated measurements.

number of passes and applied pressure. In principle, higher nanoparticle concentrations should aid the formation of finer droplets because more nanoparticles are available to stabilize the additional droplet surface area generated during microfluidization. The PGMA₄₈-PTFEMA₅₀ concentration in the precursor macroemulsion was adjusted from 1.0 to 7.0% w/w (Figure 3).

A significant reduction in mean droplet diameter (and DLS polydispersity) was achieved for PGMA₄₈-PTFEMA₅₀ concentrations ranging from 1.0 to 5.0% w/w. However, using higher concentrations under such conditions did not lead to droplets smaller than 200 nm diameter.

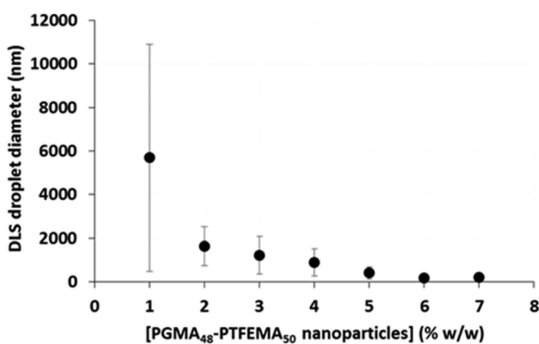


Figure 3. Variation in the intensity-average droplet diameter with nanoparticle concentration for an *n*-dodecane volume fraction of 0.20, a constant applied pressure of 20 000 psi, and ten passes through an LV1 microfluidizer. Error bars represent standard deviations for the DLS droplet size distributions rather than the experimental error associated with repeated measurements.

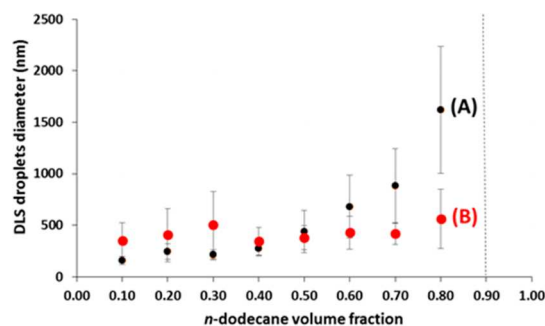


Figure 4. Effect of varying the *n*-dodecane volume fraction on the mean droplet diameter of the resulting Pickering nanoemulsion after 10 passes through an LV1 microfluidizer at a constant applied pressure of 20 000 psi. (A) The nanoparticle concentration in the aqueous phase was held constant at 7.0% w/w and (B) the total nanoparticle concentration in the overall emulsion was held constant at 5.7% w/w. Error bars represent the standard deviations of the DLS droplet size distributions rather than the experimental error associated with repeated measurements.

Varying the *n*-Dodecane Volume Fraction. Figure 4 shows the effect of varying the *n*-dodecane volume fraction from 0.10 to 0.90. This was achieved by two methods. First, the PGMA₄₈-PTFEMA₅₀ concentration in the aqueous phase was fixed at 7.0% w/w, hence the overall nanoparticle concentration in the final emulsion was gradually reduced on increasing the oil volume fraction (Figure 4A). The mean droplet diameter gradually increased from 160 nm at an oil volume fraction of 0.10 up to 1620 nm for an oil volume fraction of 0.80. Progressively larger oil droplets were obtained up to the point where no more oil could be processed via microfluidization: utilizing an oil volume fraction of 0.90 led to no reduction in droplet size relative to the volume-average diameter of 47 μ m obtained for the precursor Pickering macroemulsion via high-shear homogenization. In an alternative approach, the nanoparticle concentration in the aqueous phase was systematically varied while increasing the *n*-dodecane volume fraction such that the overall nanoparticle concentration in the formulated emulsion remained constant (Figure 4B). This strategy resulted in a relatively constant intensity-average droplet diameter of 400 to 500 nm for oil volume fractions of up to 0.80. This was expected because the overall nanoparticle concentration was the same for each emulsion. It is noteworthy that a high internal phase emulsion (HIPE) could be achieved in both cases, with the latter strategy yielding a HIPE comprising relatively fine droplets of 560 \pm 290 nm. Moreover, no phase inversion was observed at high oil volume fractions. We attribute this to the highly hydrophilic nature of the PGMA stabilizer chains, which makes it rather unlikely that such nanoparticles could stabilize water-in-oil emulsions.

TEM Analysis of Dried Nanoemulsion Droplets. We have previously reported that various linear diblock copolymer nanoparticles can undergo in situ dissociation to form molecularly dissolved copolymer chains under the high-shear homogenization conditions utilized for emulsification.^{35,36} Stable emulsions can still be obtained under such conditions, but they are not genuine Pickering emulsions because the original nanoparticle morphology is lost. Thus, in the present work it was important to examine whether the PGMA₄₈-PTFEMA₅₀ nanoparticles actually survive the processing conditions intact. Accordingly, a dried Pickering nanoemulsion prepared at 20 000 psi was imaged by TEM using a uranyl formate negative stain to improve the electron contrast (Figure 5). This particular nanoemulsion had an intensity-average diameter of 220 \pm 85 nm as judged by DLS. The superstructure of these nanoparticles (which possess a number-average diameter of approximately 20 nm as judged by TEM analysis) is clearly preserved on drying the nanoemulsion droplets (see inset image), indicating that microfluidization at 20 000 psi does not result in the loss of the original nanoparticle morphology. In contrast, when imaging a dried nanoemulsion prepared using the same nanoparticles at 30 000 psi, there is little or no evidence for the

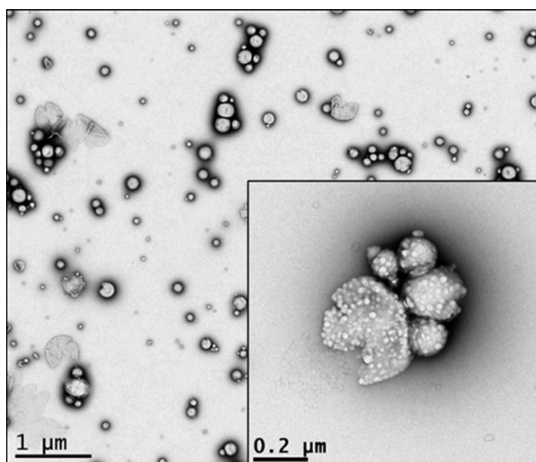


Figure 5. Representative TEM images obtained for dried *n*-dodecane-in-water Pickering nanoemulsions stabilized using 7.0% w/w PGMA₄₈-PTFEMA₅₀ nanoparticles at a microfluidizer pressure of 20 000 psi. Nine passes were employed, which produced a Pickering nanoemulsion with an intensity-average droplet diameter of 220 ± 85 nm.

original spherical morphology (Figure S5A). Presumably, this nanoemulsion is stabilized by individual copolymer chains acting as a polymeric surfactant and hence cannot be considered to be a genuine Pickering nanoemulsion. Clearly, there is an upper-limit microfluidization pressure (>20 000 psi) beyond which nanoparticle dissociation occurs. In principle, this problem can be overcome by using cross-linked nanoparticles. Indeed, preliminary experiments performed using such covalently stabilized nanoparticles at 30 000 psi produced genuine Pickering nanoemulsions (Figure S5B in Supporting Information), although no further reduction in droplet diameter could be achieved under these conditions.

Attempted Use of Larger Nanoparticles to Prepare Pickering Nanoemulsions. Using larger PGMA₄₈-PTFEMA₁₅₀ nanoparticles of 51 nm diameter invariably led to flocculated macroemulsions, with DLS studies reporting apparent droplet diameters of more than $1 \mu\text{m}$ (Figure S6A). Such aggregation was always observed, despite using nanoparticle concentrations of up to 19% w/w to compensate for the reduction in the specific surface area of these larger nanoparticles. TEM studies of the dried flocculated emulsions confirmed that they comprised aggregates of submicrometer-sized droplets (Figure S6B). One possible explanation for such aggregation may be slower adsorption kinetics for these larger nanoparticles during microfluidization. This would produce a lower initial droplet coverage and hence could lead to a particle-bridging mechanism.⁴¹

Packing of Small Spheres around a Large Sphere. Pickering emulsions usually involve either close-packed shells of particles²⁵ or relatively thick multilayers of flocculated particles,³ although there are a few literature examples of stable emulsion droplets being obtained at relatively low surface coverage.^{42,43} Our TEM observations suggest the formation of close-packed nanoparticle monolayers (Figure 5), so we wished to investigate the fractional surface coverage of nanoparticles for this new class of Pickering nanoemulsions. Accordingly, in this section we calculate mathematical estimates of the maximum number of spheres that can surround a larger sphere with a given radius ratio as a model for the nanoparticle-coated oil droplets reported in this work.

DLS can be used to determine the mean radius, r_v , for the spherical nanoparticles prior to any emulsification. The same technique also yields a mean overall (total) radius, r_t , for the nanoparticle-coated oil droplets. Consider such a droplet comprising a spherical liquid (oil) core of radius r_1 coated with spherical nanoparticles (Figure 6). Assuming hard-sphere contacts between the two components, the relationship between r_1 and r_t is given by

$$r_1 = r_t - 2r_s \quad (1)$$

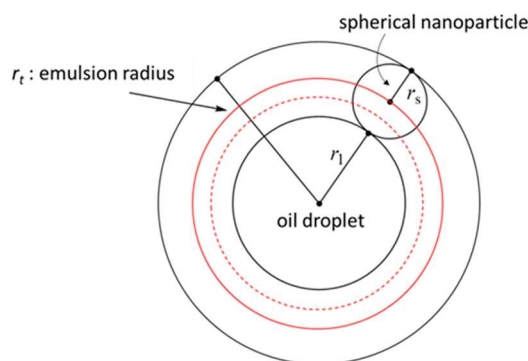


Figure 6. Packing of small nanoparticles of radius r_s around a spherical oil droplet of radius r_1 . The overall (total) droplet radius, r_t , is given by $r_t = r_1 + 2r_s$, as in eq 1. DLS enables separate determination of both r_t and r_s .

As Figure 6 shows, this equation corresponds to the situation where nanoparticles of radius r_s are packed on the inside surface of a limiting sphere of radius r_t , affording a minimum inner droplet radius r_1 (inner black circle in Figure 6); this is the radius used in the packing calculations (see below). The solid red line in Figure 6 represents the theoretical maximum droplet radius ($r_1 + r_s$) corresponding to a liquid-particle contact angle of 90° . The true extent to which the nanoparticles are wetted by the oil phase (qualitatively indicated by the red dashed line) presumably lies somewhere between these limits, with an effective particle contact angle lying between 0 and 90° .

Various radius ratios (r_s/r_1) calculated using eq 1 are listed in Table 1. For $r_s = 12.5$ nm, the corresponding r_t values in Table 1 were

Table 1. Summary of r_s , r_t , and r_1 Values and the Corresponding Radius Ratios (r_s/r_1) Calculated Using Equation 1 for Both Experimental (Entries 1–3) and Hypothetical (Entries 4–6) Pickering Nanoemulsions^a

entry	r_s/nm	r_t/nm	r_1/nm	r_s/r_1
1	12.5	66.5	41.5	0.30
2	12.5	110.0	85.0	0.15
3	12.5	245.0	220.0	0.06
4	25.5	66.5	15.5	1.65
5	25.5	110.0	59.0	0.43
6	25.5	245.0	194.0	0.13

^aSee the text for further details.

determined for nanoemulsions using DLS (entries 1–3). However, for $r_s = 25.5$ nm, only aggregated emulsions could be obtained experimentally, and there are no corresponding r_t values for entries 4–6. Therefore, we took the r_t values measured for entries 1–3 and calculated the corresponding r_1 values for hypothetical droplets from eq 1. The radius ratios listed in this table were used to estimate the maximum number of nanoparticles of radius r_s that can be packed around a central oil droplet of radius r_1 .

Packing N spheres around a central (usually larger) sphere is mathematically equivalent to solving a circle-packing problem of finding the maximum radius of the smaller spheres that is allowed if N smaller spheres are packed around the central large sphere. If the radii of the central and packed spheres are r_1 and r_s , respectively, then the points of tangential contact between the packed spheres lie on a sphere of radius $(r_1 + r_s)\cos r_c$, where r_c is the angular radius of the equivalent circular cap in a packing of N circles on a sphere of unit radius (Figure 7). This dimensionless cap radius is given by

$$r_c = \sin^{-1}\left(\frac{r_s}{r_1 + r_s}\right) \quad (2)$$

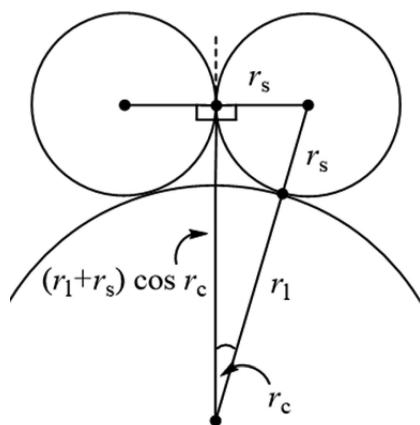


Figure 7. Schematic representation of the geometric considerations involved in the packing of N small spheres around a large central sphere.

The radius ratio for the sphere packing problem (r_s/r_1) is then related to the angle r_c by eq 3

$$\frac{r_s}{r_1} = \sin \frac{r_c}{1 - \sin r_c} \quad (3)$$

The packing density, P , can be calculated from N and r_c , where r_c is an implicit function of N , as

$$P = \frac{1}{2}N(1 - \cos r_c) = N \sin^2 \left(\frac{r_c}{2} \right) \quad (4)$$

By definition, for any fixed N there is a maximum r_c (the packing radius) and corresponding packing density P , with $0 \leq P \leq 1$. The full range of P is not physically accessible. For example, a perfect hexagonal lattice of circles achieves $P = \pi\sqrt{12} \approx 0.9069$, but even this hard upper limit cannot be achieved for a sphere because some packing defects or scars must exist to allow for spherical curvature.⁴⁴

A proven optimal solution is known for only a few values of N . In all of these cases, the corresponding packing density is substantially below the hexagonal packing limit. However, computational results are available. Sloane et al.^{45,46} give tables of best known packings for two cases. In the first case, the table⁴⁵ is for all N values lying between 4 and 130 and is based on extensive calculations without the restriction of symmetry. The results match known exact solutions and in other cases they are expected to lie close to the exact value for the given N . Sloane et al. also list computed solutions for large values of N and packings restricted to icosahedral symmetry,⁴⁶ which give a mesh of empirical lower bounds for particular values of N . All results obtained using this approach indicate packing densities substantially below the hexagonal-packing upper bound.

Scatterplots of the data obtained from these two tabulations are given in Figure S7. Figure S7A shows the relationship between the number of packed spheres and the radius ratio. As N is increased,^{45,46}

the maximum radius ratio that can be achieved tends smoothly toward zero. Figure S7B translates these data into a plot of packing density P against N . The data up to $N = 130$ suggest that P approaches a limiting value of ~ 0.84 . The smooth variation in packing density for experimentally realistic N values is consistent with the small dispersion in various mathematical estimates, as shown in Table 2.

There are reliable theoretical upper⁴⁷ and lower^{48,49} bounds on N in terms of the radius ratio.⁵⁰ The results are summarized in Table 2, along with our own ad hoc estimates based on interpolation of Sloane's tables and reasonable assumptions for typical packing densities. We note that the $N(85)$ values, calculated assuming a packing density of 0.85 (85%), are close to those interpolated from Sloane's tables^{41,42} and from a spiral construction.⁴⁹ Given the agreement between the various approaches, the values of $N(\text{Sloane})$ given in Table 2 are plausible estimates for the number of nanoparticles packed around each oil droplet.

In the experiments associated with entry 1, a colloidally stable nanoemulsion was obtained, but a relatively high pressure (30 000 psi) was required to generate the small r_t value indicated by DLS. The data presented in Table 2 suggests that in a packed morphology approximately 60–64 nanoparticles should be present, but TEM analysis of this nanoemulsion showed no evidence of the original nanoparticles (Figure S5). This indicates that the nanoparticles do not survive these high-pressure microfluidization conditions. Thus, this entry most probably corresponds not to a true Pickering nanoemulsion but to a nanoemulsion stabilized by individual copolymer chains. In contrast, the microfluidization experiments indicated by entries 2 and 3 produced stable nanoparticle-coated droplets, as confirmed by TEM studies. For example, in the case of entry 2, TEM analysis provides clear evidence for adsorbed intact nanoparticles (Figure 5). Moreover, the N values calculated in Table 2 appear to be physically realistic (approximately 200 nanoparticles packed around each oil droplet). For experiments performed using larger nanoparticles ($r_s = 25.5$ nm), DLS and TEM studies indicated that only aggregated oil droplets could be obtained, with intact nanoparticles adsorbed at the interface (Figure S5B).

The N values shown in Table 2 (see entry 6) are consistent with TEM analysis, but it also appears that additional as-yet-unidentified physical factors affect the degree of dispersion of this particular Pickering nanoemulsion.

When connecting the circle-packing model to the physical situation of nanoparticle-coated oil droplets, additional factors may be involved. For example, there will be a repulsive interaction between adjacent packed nanoparticles, but it may be softer than the assumed hard sphere model. Thus, it is feasible that the effective nanoparticle radius corresponding to the repulsive pair potential may be larger than that determined using DLS. Moreover, efficient nanoparticle packing corresponds to a global optimum N value for a given effective contact radius. If the nanoparticles are irreversibly adsorbed at the oil/water interface, have low mobility on the oil droplet surface, or interact with each other to generate specific local patterns, then the number of surface nanoparticles may be lower than the mathematical optimum. This may explain why colloidally stable Pickering nanoemulsions could not be obtained when using the larger nanoparticles (i.e., for $r_s = 25.5$

Table 2. Summary of the Numbers of Packed Spheres, N , Calculated for Six Pairs of Radii^a

entry	r_s/nm	r_t/nm	r_c/radian	N (Robinson)	N (Sloane)	N (spiral)	N (vdW)	$N(85)$	$N(80)$
1	12.5	66.5	0.23	64	61	59	33	63	59
2	12.5	110.0	0.13	217	200	198	142	206	193
3	12.5	245.0	0.05	1251	1172	1171	1006	1175	1106
4	25.5	66.5	0.67	6	7	6	2	8	7
5	25.5	110.0	0.31	37	36	37	16	36	34
6	25.5	245.0	0.12	265	240	240	179	251	236

^a $N(\text{Robinson})$ and $N(\text{vdW})$ are mathematical upper and lower bounds. $N(\text{spiral})$ is a lower bound based on the explicit construction of a spiral packing⁴⁹ and improves for the conservative van der Waerden⁴⁸ (vdW) lower bound in all cases. $N(\text{Sloane})$ is derived by us from Sloane's tables^{41,42} by taking the largest value of N with a radius ratio strictly greater than the given experimental ratio. In the final two columns, $N(85)$ and $N(80)$ are estimated by assuming fixed packing densities of 85 and 80%, respectively. All values are rounded to the nearest integer.

nm; see entries 4–6 in Table 2), despite packing calculations suggesting that this should be theoretically possible at least for entry 6. For these larger nanoparticles, other physical factors such as their slower diffusion to the oil/water interface and stronger adsorption at this interface may favor particle bridging and limit their ability to form well-dispersed oil droplets.

Long-Term Stability Studies. Various literature reports indicate that Oswald ripening typically leads to droplet coarsening and/or coalescence for aged nanoemulsions.^{5,11,51} Such instability is well-documented even for relatively water-insoluble oils such as *n*-alkanes. However, these new Pickering nanoemulsions exhibit good long-term colloidal stability: visual inspection indicated no signs of phase separation, and DLS studies confirmed that the original droplet size distribution remained almost unchanged on storing these Pickering nanoemulsions at room temperature for approximately 4 months (Figure 8). This suggests that the 25 nm sterically stabilized PGMA₄₈-PTFEMA₅₀ nanoparticles used in the present work are adsorbed rather more strongly at the oil/water interface than the 7 nm charge-stabilized silica nanoparticles reported by Persson et al.⁵

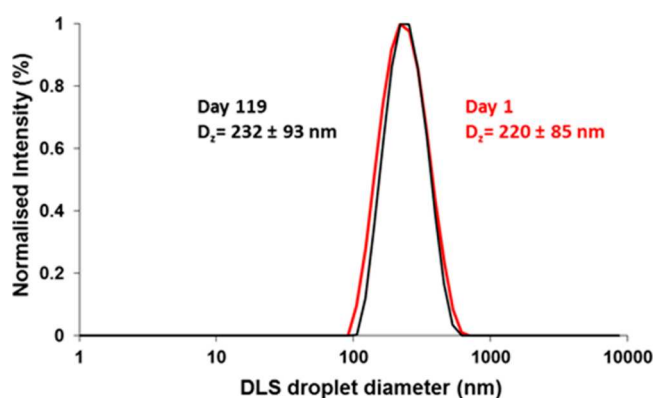


Figure 8. Droplet size distributions determined by dynamic light scattering for a freshly prepared Pickering nanoemulsion stabilized using PGMA₄₈-PTFEMA₅₀ nanoparticles and again after standing at 20 °C for 119 days. The negligible change in the intensity-average droplet diameter and polydispersity indicates excellent long-term stability against droplet coalescence via Ostwald ripening.

CONCLUSIONS

In summary, diblock copolymer nanoparticles have been used to stabilize oil-in-water Pickering nanoemulsions for the first time. Direct evidence for the presence of intact nanoparticles adsorbed at the droplet surface is provided by TEM studies of the dried nanoemulsion. This is consistent with model calculations based on radius ratios, which suggest a relatively high nanoparticle packing density for nanoemulsion droplets with an overall mean DLS diameter of 220 nm.

Our approach offers the following decisive advantages: (i) the absence of any other additives, (ii) use of a scalable emulsification technology to achieve fine control over the mean droplet diameter, and (iii) enhanced long-term droplet stability toward Ostwald ripening, even for oils exhibiting finite water solubility such as *n*-dodecane.

ASSOCIATED CONTENT

Supporting Information

The Supporting Information is available free of charge on the ACS Publications website at DOI: 10.1021/acs.langmuir.7b02267.

GPC analysis of PGMA₄₈-PTFEMA₅₀ copolymer chains; additional DLS data for copolymer nanoparticles and

Pickering (nano)emulsions; additional laser diffraction data for Pickering emulsions; digital photographs of Pickering (nano)emulsions; additional TEM images of dried nanoemulsion droplets; mathematical relationships between (i) the radius ratio and *N* and (ii) the packing density and *N*, where *N* is the number of nanoparticles packed around a single oil droplet. (PDF)

AUTHOR INFORMATION

Corresponding Authors

*E-mail: kate.thompson@manchester.ac.uk.

*E-mail: s.p.armes@shef.ac.uk.

ORCID

Steven P. Armes: 0000-0002-8289-6351

Notes

The authors declare no competing financial interest.

ACKNOWLEDGMENTS

S.P.A. thanks EPSRC (platform grant EP/J007846/1) and also acknowledges a five-year Advanced Investigator ERC grant (PISA 320372).

REFERENCES

- Pickering, S. U. Emulsions. *J. Chem. Soc., Trans.* **1907**, *91*, 2001–2021.
- Ramsden, W. Separation of Solids in the Surface-Layers of Solutions and 'Suspensions' (Observations on Surface-Membranes, Bubbles, Emulsions, and Mechanical Coagulation). – Preliminary Account. *Proc. R. Soc. London* **1903**, *72*, 156–164.
- Binks, B. P. Particles as surfactants - similarities and differences. *Curr. Opin. Colloid Interface Sci.* **2002**, *7*, 21–41.
- Tadros, T.; Izquierdo, R.; Esquena, J.; Solans, C. Formation and stability of nano-emulsions. *Adv. Colloid Interface Sci.* **2004**, *108-109*, 303–318.
- Persson, K. H.; Blute, I. A.; Mira, I. C.; Gustafsson, J. Creation of well-defined particle stabilized oil-in-water nanoemulsions. *Colloids Surf., A* **2014**, *459*, 48–57.
- Sonneville-Aubrun, O.; Simonnet, J. T.; L'Alloret, F. Nano-emulsions: a new vehicle for skincare products. *Adv. Colloid Interface Sci.* **2004**, *108-109*, 145–149.
- Rapoport, N. Y.; Kennedy, A. M.; Shea, J. E.; Scaife, C. L.; Nam, K.-H. Controlled and targeted tumor chemotherapy by ultrasound-activated nanoemulsions/microbubbles. *J. Controlled Release* **2009**, *138*, 268–276.
- McClements, D. J.; Rao, J. Food-Grade Nanoemulsions: Formulation, Fabrication, Properties, Performance, Biological Fate, and Potential Toxicity. *Crit. Rev. Food Sci. Nutr.* **2011**, *51*, 285–330.
- Ugelstad, J.; El-Aasser, M. S.; Vanderhoff, J. W. Emulsion polymerization: Initiation of polymerization in monomer droplets. *J. Polym. Sci., Polym. Lett. Ed.* **1973**, *11*, 503–513.
- Tiarks, F.; Landfester, K.; Antonietti, M. Silica Nanoparticles as Surfactants and Fillers for Latexes Made by Miniemulsion Polymerization. *Langmuir* **2001**, *17*, 5775–5780.
- Du, Z.; Wang, C.; Tai, X.; Wang, G.; Liu, X. Optimization and Characterization of Biocompatible Oil-in-Water Nanoemulsion for Pesticide Delivery. *ACS Sustainable Chem. Eng.* **2016**, *4*, 983–991.
- Santos, J.; Trujillo-Cayado, L. A.; Calero, N.; Alfaro, M. C.; Munoz, J. Development of eco-friendly emulsions produced by microfluidization technique. *J. Ind. Eng. Chem.* **2016**, *36*, 90–95.
- Solans, C.; Izquierdo, P.; Nolla, J.; Azemar, N.; Garcia-Celma, M. J. Nano-emulsions. *Curr. Opin. Colloid Interface Sci.* **2005**, *10*, 102–110.
- Gupta, A.; Eral, H. B.; Hatton, T. A.; Doyle, P. S. Nanoemulsions: formation, properties and applications. *Soft Matter* **2016**, *12*, 2826–2841.

- (15) Izquierdo, P.; Esquena, J.; Tadros, T. F.; Dederen, C.; Garcia, M. J.; Azemar, N.; Solans, C. Formation and stability of nano-emulsions prepared using the phase inversion temperature method. *Langmuir* **2002**, *18*, 26–30.
- (16) Izquierdo, P.; Esquena, J.; Tadros, T. F.; Dederen, J. C.; Feng, J.; Garcia-Celma, M. J.; Azemar, N.; Solans, C. Phase Behavior and nano-emulsion formation by the phase inversion temperature method. *Langmuir* **2004**, *20*, 6594–6598.
- (17) Gupta, A.; Badruddoza, A. Z. M.; Doyle, P. S. A General Route for Nanoemulsion Synthesis Using Low-Energy Methods at Constant Temperature. *Langmuir* **2017**, *33*, 7118–7123.
- (18) Forgiarini, A.; Esquena, J.; Gonzalez, C.; Solans, C. Formation of nano-emulsions by low-energy emulsification methods at constant temperature. *Langmuir* **2001**, *17*, 2076–2083.
- (19) Sacanna, S.; Kegel, W. K.; Philipse, A. P. Thermodynamically Stable Pickering Emulsions. *Phys. Rev. Lett.* **2007**, *98*, 158301.
- (20) Sihler, S.; Schrade, A.; Cao, Z.; Ziener, U. Inverse Pickering Emulsions with Droplet Sizes below 500 nm. *Langmuir* **2015**, *31*, 10392–10401.
- (21) Cheong, A. M.; Tan, K. W.; Tan, C. P.; Nyam, K. L. Kenaf (*Hibiscus cannabinus* L.) seed oil-in-water Pickering nanoemulsions stabilised by mixture of sodium caseinate, Tween 20 and β -cyclodextrin. *Food Hydrocolloids* **2016**, *52*, 934–941.
- (22) Sadeghpour, A.; Pirolt, F.; Glatter, O. Submicrometer-Sized Pickering Emulsions Stabilized by Silica Nanoparticles with Adsorbed Oleic Acid. *Langmuir* **2013**, *29*, 6004–6012.
- (23) Warren, N. J.; Armes, S. P. Polymerization-Induced Self-Assembly of Block Copolymer Nano-objects via RAFT Aqueous Dispersion Polymerization. *J. Am. Chem. Soc.* **2014**, *136*, 10174–10185.
- (24) Cunningham, V. J.; Alswieleh, A. M.; Thompson, K. L.; Williams, M.; Leggett, G. J.; Armes, S. P.; Musa, O. M. Poly(glycerol monomethacrylate)-Poly(benzyl methacrylate) Diblock Copolymer Nanoparticles via RAFT Emulsion Polymerization: Synthesis, Characterization, and Interfacial Activity. *Macromolecules* **2014**, *47*, 5613–5623.
- (25) Rymaruk, M. J.; Thompson, K. L.; Derry, M. J.; Warren, N. J.; Ratcliffe, L. P. D.; Williams, C. N.; Brown, S. L.; Armes, S. P. Bespoke contrast-matched diblock copolymer nanoparticles enable the rational design of highly transparent Pickering double emulsions. *Nanoscale* **2016**, *8*, 14497–14506.
- (26) Sun, J. T.; Hong, C. Y.; Pan, C. Y. Recent advances in RAFT dispersion polymerization for preparation of block copolymer aggregates. *Polym. Chem.* **2013**, *4*, 873–881.
- (27) Zhang, W.; D'Agosto, F.; Boyron, O.; Rieger, J.; Charleux, B. Toward Better Understanding of the Parameters that Lead to the Formation of Nonspherical Polystyrene Particles via RAFT-Mediated One-Pot Aqueous Emulsion Polymerization. *Macromolecules* **2012**, *45*, 4075–4084.
- (28) Dinsmore, A. D.; Hsu, M. F.; Nikolaidis, M. G.; Marquez, M.; Bausch, A. R.; Weitz, D. A. Colloidosomes: Selectively permeable capsules composed of colloidal particles. *Science* **2002**, *298*, 1006–1009.
- (29) Cayre, O. J.; Noble, P. F.; Paunov, V. N. Fabrication of novel colloidosome microcapsules with gelled aqueous cores. *J. Mater. Chem.* **2004**, *14*, 3351–3355.
- (30) Cayre, O. J.; Hitchcock, J.; Manga, M. S.; Fincham, S.; Simoes, A.; Williams, R. A.; Biggs, S. pH-responsive colloidosomes and their use for controlling release. *Soft Matter* **2012**, *8*, 4717–4724.
- (31) Thompson, K. L.; Armes, S. P.; Howse, J. R.; Ebbens, S.; Ahmad, I.; Zaidi, J. H.; York, D. W.; Burdis, J. A. Covalently Cross-Linked Colloidosomes. *Macromolecules* **2010**, *43*, 10466–10474.
- (32) Subramaniam, A. B.; Abkarian, M.; Stone, H. A. Controlled assembly of jammed colloidal shells on fluid droplets. *Nat. Mater.* **2005**, *4*, 553–556.
- (33) Blanazs, A.; Madsen, J.; Battaglia, G.; Ryan, A. J.; Armes, S. P. Mechanistic Insights for Block Copolymer Morphologies: How do Worms Form Vesicles? *J. Am. Chem. Soc.* **2011**, *133*, 16581–16587.
- (34) Akpınar, B.; Fielding, L. A.; Cunningham, V. J.; Ning, Y.; Mykhaylyk, O. O.; Fowler, P. W.; Armes, S. P. Determining the Effective Density and Stabilizer Layer Thickness of Sterically Stabilized Nanoparticles. *Macromolecules* **2016**, *49*, 5160–5171.
- (35) Thompson, K. L.; Chambon, P.; Verber, R.; Armes, S. P. Can Polymersomes Form Colloidosomes? *J. Am. Chem. Soc.* **2012**, *134*, 12450–12453.
- (36) Thompson, K. L.; Mable, C. J.; Cockram, A.; Warren, N. J.; Cunningham, V. J.; Jones, E. R.; Verber, R.; Armes, S. P. Are block copolymer worms more effective Pickering emulsifiers than block copolymer spheres? *Soft Matter* **2014**, *10*, 8615–8626.
- (37) Boisse, S.; Rieger, J.; Belal, K.; Di-Cicco, A.; Beaunier, P.; Li, M.-H.; Charleux, B. Amphiphilic block copolymer nano-fibers via RAFT-mediated polymerization in aqueous dispersed system. *Chem. Commun.* **2010**, *46*, 1950–1952.
- (38) Boissé, S.; Rieger, J.; Pembouong, G.; Beaunier, P.; Charleux, B. Influence of the stirring speed and CaCl₂ concentration on the nano-object morphologies obtained via RAFT-mediated aqueous emulsion polymerization in the presence of a water-soluble macroRAFT agent. *J. Polym. Sci., Part A: Polym. Chem.* **2011**, *49*, 3346–3354.
- (39) Rizzardo, E.; Solomon, D. A new method for investigating the mechanism of initiation of radical polymerization. *Polym. Bull.* **1979**, *1*, 529–534.
- (40) Binks, B. P.; Lumsdon, S. O. Pickering emulsions stabilized by monodisperse latex particles: Effects of particle size. *Langmuir* **2001**, *17*, 4540–4547.
- (41) Horozov, T. S.; Binks, B. P. Particle-Stabilized Emulsions: A Bilayer or a Bridging Monolayer? *Angew. Chem., Int. Ed.* **2006**, *45*, 773–776.
- (42) Vignati, E.; Piazza, R.; Lockhart, T. P. Pickering Emulsions: Interfacial Tension, Colloidal Layer Morphology, and Trapped-Particle Motion. *Langmuir* **2003**, *19*, 6650–6656.
- (43) Gautier, F.; Destribats, M.; Perrier-Cornet, R.; Dechezelles, J.-F.; Giermanska, J.; Heroguez, V.; Ravaine, S.; Leal-Calderon, F.; Schmitt, V. Pickering emulsions with stimutable particles: from highly- to weakly-covered interfaces. *Phys. Chem. Chem. Phys.* **2007**, *9*, 6455–6462.
- (44) Bausch, A. R.; Bowick, M. J.; Cacciuto, A.; Dinsmore, A. D.; Hsu, M. F.; Nelson, D. R.; Nikolaidis, M. G.; Travesset, A.; Weitz, D. A. Grain Boundary Scars and Spherical Crystallography. *Science* **2003**, *299*, 1716–1718.
- (45) Sloane, N. J. A.; Hardin, R. H.; Smith, W. D. et al. *Spherical Codes*; published electronically at NeilSloane.com/packings/; accessed February 24, 2017.
- (46) Hardin, R. H.; Sloane, N. J. A.; Smith, W. D. *Tables of Spherical Codes with Icosahedral Symmetry*; published electronically at <http://neilsloane.com/icosahedral.codes/>; accessed February 24, 2017.
- (47) Robinson, R. M. Arrangement of 24 points on a sphere. *Mathematische Annalen* **1961**, *144*, 17–48.
- (48) van der Waerden, B. L. Punkte auf der Kugel. Drei Zusätze. *Mathematische Annalen* **1952**, *125*, 213–222.
- (49) Gáspár, Z. Spiral circle packings on a sphere. *Ann. Univ. Sci. Bpest. Rolando Eötvös Sect. Math.* **1990**, *33*, 61–74.
- (50) Balmer, J. A.; Armes, S. P.; Fowler, P. W.; Tarnai, T.; Gaspar, Z.; Murray, K. A.; Williams, N. S. J. Packing Efficiency of Small Silica Particles on Large Latex Particles: A Facile Route to Colloidal Nanocomposites. *Langmuir* **2009**, *25*, 5339–5347.
- (51) Ali, A.; Mekhloufi, G.; Huang, N.; Agnely, F. beta-lactoglobulin stabilized nanemulsions-Formulation and process factors affecting droplet size and nanoemulsion stability. *Int. J. Pharm.* **2016**, *500*, 291–304.